Supporting Information for

Halogen bonding-assembled hybrid copper halide framework for promising hypotoxicity photodetector

Guang-Ning Liu,*[,a] Ming-Kun Li,[a] Rang-Dong Xu,[a] Ning-Ning Zhang,[b] Xin-Jiao Quan,[a] Bing-Jing Qian,[a] Yi-Han Lu,[a] and Cuncheng Li[a]

[a]*School of Chemistry and Chemical Engineering, University of Jinan, Jinan Shandong 250022, PR China*

[b]*College of Chemistry and Chemical Engineering, Liaocheng University, Liaocheng, 252059, PR China*

Contents

S1 Experimental Section

S1.1 Material and characterization

All reagents were purchased commercially and used without further purification. CuI (99%), KI (99.5%), 5-chloropyridine-2-thiol (95%) were provided by Macklin. Hydroiodic acid (45%) was purchased from Shanghai Kefeng Chemical Regent Co., Ltd. Ethanol and acetonitrile were purchased from Sinopharm Chemical Regent Co. Elemental analyses of C, H, and N were performed on an Elementar Vario EL III microanalyzer. Powder X-ray diffraction (PXRD) patterns were recorded on Rigaku SmartlabSE diffractometer using Cu $K\alpha$ radiation. A TA instrument Q500 thermo gravimetric analyzer was used to obtain the thermogravimetric analyses (TGA) curve in N_2 with a flow rate of 20 mL·min^{-1} and a ramp rate of 10 °C·min^{-1} in the temperature range 40–800 °C. An empty Al_2O_3 crucible was used as the reference. The FT-IR spectra were obtained on a Perkin-Elmer spectrophotometer using KBr disk in the range 4000–450 cm^{-1}. Optical diffuse reflectance spectra were measured at room temperature with a Shimadzu UV-3600 Plus UV-vis spectrophotometer. The instrument was equipped with an integrating sphere and controlled with a personal computer. The samples were ground into fine powder and pressed onto a thin glass slide holder. A $BaSO_4$ plate was used as a standard (100% reflectance). The absorption spectra were calculated from reflectance spectrum using the Kubelka-Munk function:[1] $\alpha/S = (1\text{-}R)^2/2R$ where α is the absorption coefficient, S is the scattering coefficient, and R is the reflectance. The Hirshfeld surfaces and the corresponding finger print plots were generated using Crystal Explorer17 software.[2] The Hall measurements were performed on a Ecopia HMS-7000 machine. All test samples were fabricated as polycrystalline thin films. The temperature-dependent solid-state photoluminescence (TDPL) spectra were recorded on an Edinberg FLS920 fluorescence spectrophotometer. The integrated emission intensity was fitted using equation (1), in which I_0 is the intensity at 0 K, E_b the binding energy, and k_B the Boltzmann constant.[3]

$$I(T) = \frac{I_0}{1 + Ae^{-E_b/k_B T}} \quad (1)$$

S1.2 Synthesis of BCS-CuI

The single crystals of **BCS-CuI** were prepared by a mild solvothermal method. Typically, 0.20 mmol CuI (0.038 g), 0.27 mmol 5-chloropyridine-2-thiol (0.040 g) and 1.50 mmol KI (0.249 g) were mixed with 3 mL deionized water, 2 mL acetonitrile and 1 mL HI (45%). Then, the mixture was heated to 140 °C for 3 days. Yellow prismatic crystals and orange block crystals were obtained simultaneously. The yellow prismatic crystals of **BCS-CuI** were separated by hand with 10% yield (based on Cu).

S1.3 Computational detail

The X-ray crystallographic data of **BCS-CuI** was used to calculate its electronic structure. The calculations of density of states (DOS) were carried out using density functional theory (DFT) with one of the three nonlocal gradient-corrected exchange-correlation functionals (GGA-PBE) and performed with the CASTEP code,[4-5] which uses a plane wave basis set for the valence electrons and norm-conserving pseudopotential for the core electrons.[6] Pseudo-atomic calculations were performed for Cu $3d^{10}4s^{1}$, I $5s^{2}5p^{5}$, S $3s^{2}3p^{4}$, Cl $3s^{2}3p^{5}$, C, $2s^{2}2p^{2}$, N $2s^{2}2p^{3}$ and H $1s^{1}$. The parameters used in the calculations and convergence criteria were set by the default values of the CASTEP code.[4-5]

S1.4 Photoelectrochemical measurement

The photoelectronic tests were performed using an Au interdigital electrode. The single crystals of **BCS-CuI** (5 mg) were first grounded in an agate mortar carefully and then dispersed into 200-μL absolute ethanol to form a suspension, which were further ball milled for 30 min. After that, 3.5 μL of the well-dispersed suspension was drop-casted onto a carefully-cleaned Au electrode with a coating area of ~10 × 5 mm^2 to form a uniform thin film. Finally, the film-electrode was dried at 40 °C under a vacuum environment. For the photocurrent measurements, a 500 W Xe lamp with tunable optical power was chosen as the light source. Different band-pass filter in the range of 400–700 nm were used to get corresponding monochromatic light. All the incident intensity was adjusted with the help of a commercial optical power meter (CEL-NP2000-2) and all the electrical results were recorded by a Solartron ModuLab XM electrochemical system.

S1.5 Single-crystal structure determination

The intensity data sets were collected on a Agilent Xcalibur, Eos, Gemini CCD diffractometer equipped with a graphite-monochromated Mo K_α radiation (λ = 0.71073 Å) at 293 K. The data sets were reduced by the CrysAlisPro[7] program. An empirical absorption correction using spherical harmonics was implemented in SCALE3 ABSPACK scaling algorithm. The structures were solved by direct methods using the Siemens SHELXL package of crystallographic software.[8] Difference Fourier maps were created on the basis of these atomic positions to yield the other non-hydrogen atoms. The structures were refined using a full-matrix least-squares refinement on F^2. All non-hydrogen atoms were refined anisotropically. The hydrogen atoms were located at geometrically calculated positions and refined as riding on their parent atoms with fixed isotropic displacement parameters [U_{iso}(H) = 1.2U_{eq}(C, N)]. Crystallographic data and structural refinement are summarized in Table S1. Important bond lengths and angles are listed in Table S2.

Table S1 Crystallographic Data for BCS-CuI.

	BCS-CuI
CCDC No.	2168601
Formula	$C_{10}H_6N_2SCl_2CuI$
M_r (g mol^{-1})	447.57
Crystal system	Tetragonal
Space group	P-42$_1$m
ρ_{calcd} [g cm^{-3}]	2.130
a [Å]	18.2211(4)
b [Å]	18.2211(4)
c [Å]	4.2040(1)
α [°]	90
β [°]	90
γ [°]	90
V [Å^3]	1395.76(7)
Z	4
F (000)	848
θ range [°]	3.16–25.49
Measured reflections	11740
Independent reflections (R_{int})	1357 (R_{int} = 0.0495)
Data/params/restraints	1230/80/0
R_1[a], wR_2[b] [I>2s(I)]	0.0285, 0.0465
Goodness of fit	1.074
$\Delta\rho_{max}$ and $\Delta\rho_{min}$ [e Å^{-3}]	0.419, -0.280

[a]$R_1 = \sum||F_o|-|F_c||/\sum|F_o|$, [b]w$R_2 = \{\sum w[(F_o)^2-(F_c)^2]^2/\sum w[(F_o)^2]^2\}^{1/2}$

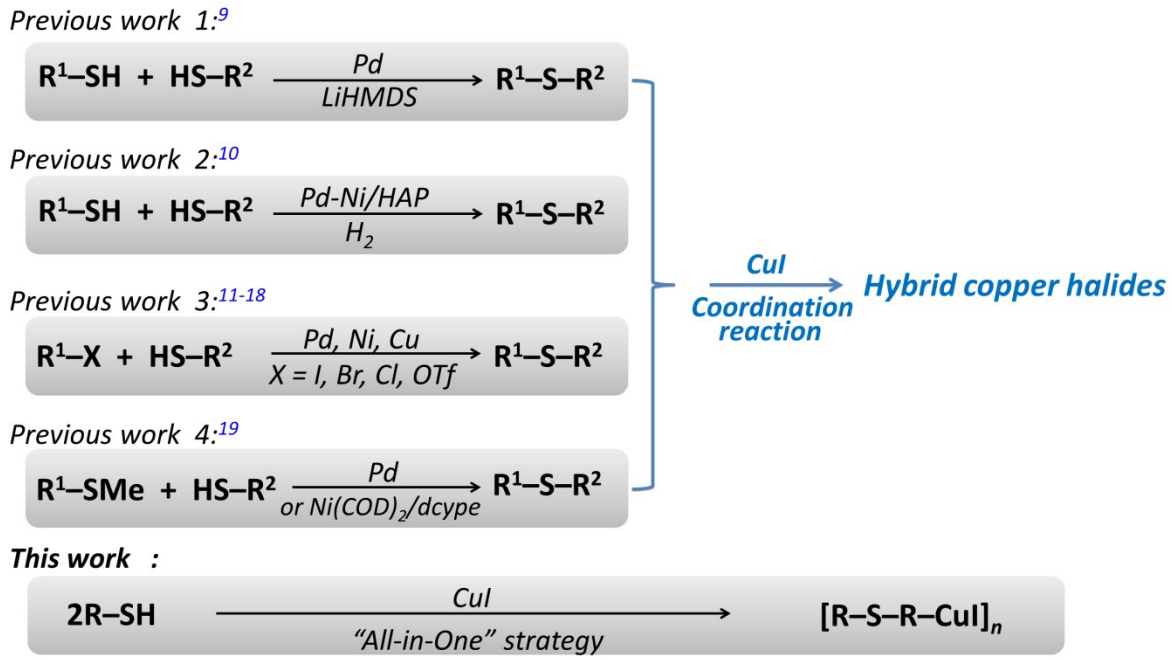

Scheme S1. Summary of previous reported C–S metathesis reactions and the "All-in-One" synthesis strategy designed in this work.

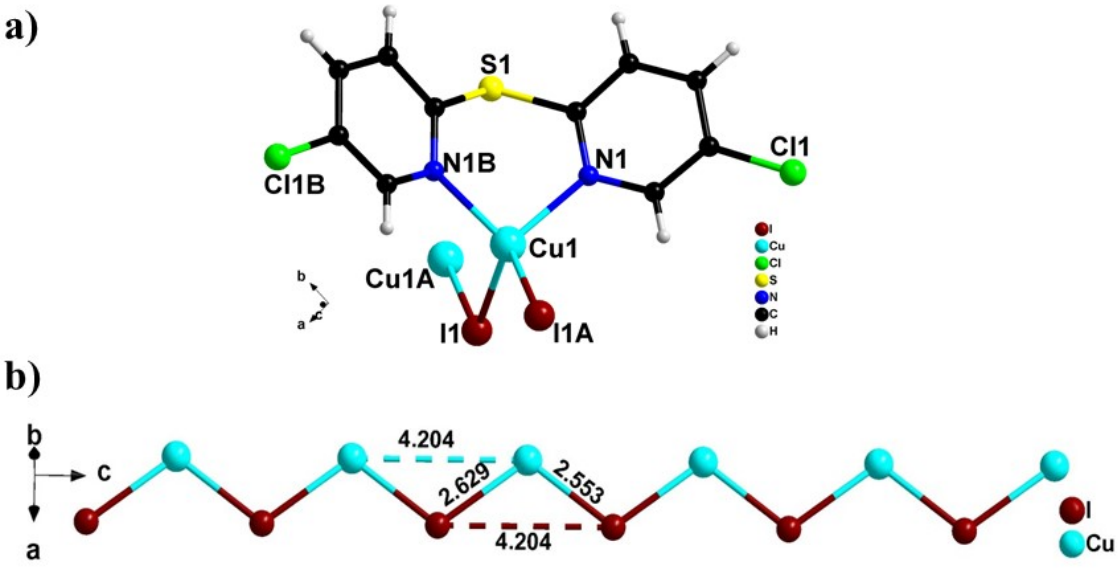

Fig. S1 (a) View of the asymmetry unit of **BCS-CuI**, symmetry code: A (x, y, -1+z) and B (1.5-y, 1.5-x, z). (b) Demonstration of the inorganic $(CuI)_n$ skeleton showing the Cu···I distances and the interval between adjacent repeating units.

Table S2 Selected Bond Distances (Å) and Angles (°) for BCS-CuI.

Bond	(Å)	Bond	(Å)
I(1)-Cu(1)	2.5536(11)	S(1)-C(5)#3	1.783(6)
I(1)-Cu(1)#1	2.6287(12)	N(1)-C(1)	1.338(7)
Cu(1)-I(1)#2	2.6288(12)	N(1)-C(5)	1.323(7)
Cu(1)-N(1)	2.057(4)	C(1)-C(2)	1.378(7)
Cu(1)-N(1)#3	2.057(4)	C(2)-C(3)	1.366(9)
Cl(1)-C(2)	1.724(7)	C(3)-C(4)	1.374(9)
S(1)-C(5)	1.783(6)	C(4)-C(5)	1.385(8)
Angle	**(°)**	**Angle**	**(°)**
Cu(1)-I(1)-Cu(1)#1	108.42(4)	C(5)-N(1)-C(1)	118.0(5)
I(1)-Cu(1)-I(1)#2	108.42(4)	N(1)-C(1)-C(2)	122.5(6)
N(1)#3-Cu(1)-I(1)#2	107.91(15)	C(1)-C(2)-Cl(1)	120.1(5)
N(1)#3-Cu(1)-I(1)	117.14(14)	C(3)-C(2)-Cl(1)	120.4(5)
N(1)-Cu(1)-I(1)	117.14(14)	C(3)-C(2)-C(1)	119.6(6)
N(1)-Cu(1)-I(1)#2	107.91(15)	C(2)-C(3)-C(4)	117.9(6)
N(1)#3-Cu(1)-N(1)	97.5(3)	C(3)-C(4)-C(5)	119.8(6)
C(5)-S(1)-C(5)#3	105.2(4)	N(1)-C(5)-S(1)	120.3(5)
C(1)-N(1)-Cu(1)	120.9(4)	N(1)-C(5)-C(4)	122.2(5)
C(5)-N(1)-Cu(1)	120.9(4)	C(4)-C(5)-S(1)	117.2(5)

Symmetry transformations used to generate equivalent atoms: #1 x, y, z+1; #2 x, y, z-1; #3 -y+3/2, -x+3/2, z.

Table S3 The C, H, and N Elemental Analyses for BCS-CuI.

BCS-CuI	C	H	N
Theoretical	26.83	1.35	6.26
Experimental	27.18	1.40	6.46

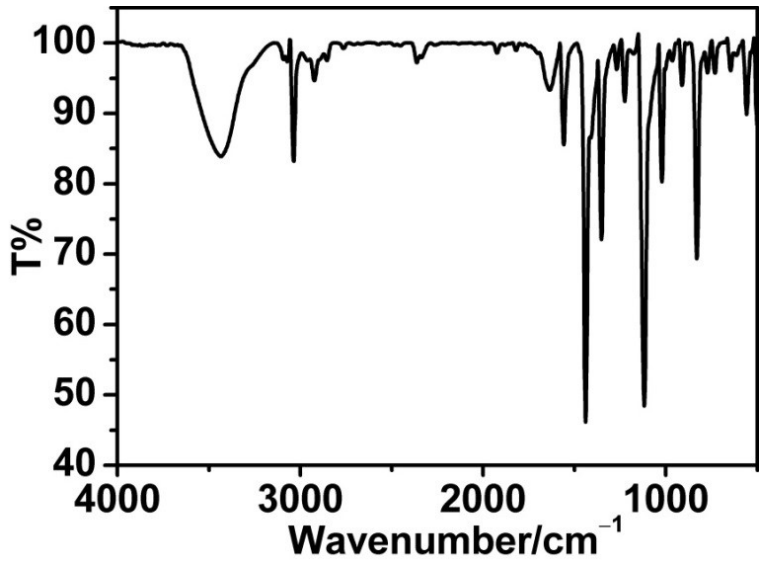

Fig. S2 IR spectrum of **BCS-CuI**.

Table S4 IR Spectral Data (KBr pellet, cm^{-1}).

Compound	**Peak position**
BCS-CuI	3433(m), 3037(m), 1634(w), 1560(m), 1440(vs), 1351(s), 1227(w), 1118(vs), 1024(m), 915(w), 830(s), 771(vw), 731(vw), 642(vw), 558(vw), 499(vw).

IR analysis: The strong peak at 3037 cm^{-1} could be ascribed to the C–H vibrations of the aromatic ring hydrogen atoms, ν(=C-H), while the bands in the range 1640–1400 cm^{-1} are assigned to the bands of ring vibrations of the conjugated ligand (ν(C=C) and ν(C=N)). Notably, the characteristic peaks of the aryl thioether appear at 1024 cm^{-1} and 642 cm^{-1} that are due to Ar–S stretching vibration. All these demonstrate the formation of the BSC molecule. The strong peak at 830 cm^{-1} could be ascribed to the C–Cl vibrations of the **BSC** molecule. The broad band at 3433 cm^{-1} is assigned to the stretching of trace water since the

measurements were conducted in air. In all, the IR results agree with the SXRD studies.

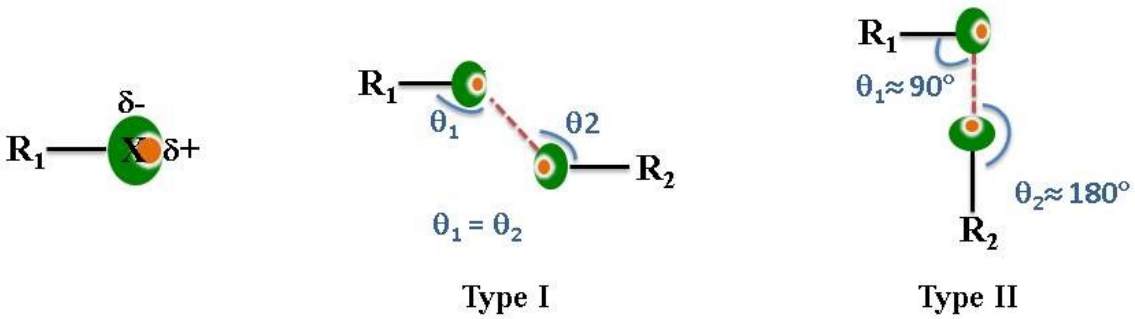

Fig. S3 Demonstration of two types of XB interactions. $\theta_1 = \theta_2$ for type-I contact, $\theta_1 \approx 90°$ and $\theta_2 \approx 180$ ° for type-II contact. The charge distribution of a halogen that bonds to an organic molecule is anisotropic. High electron density is observed around the R X–X bond axis. Lower electron density locates at cap of the halogen (also called "σ-hole"), which can be positive depending on the halogen atom and the organic rest.

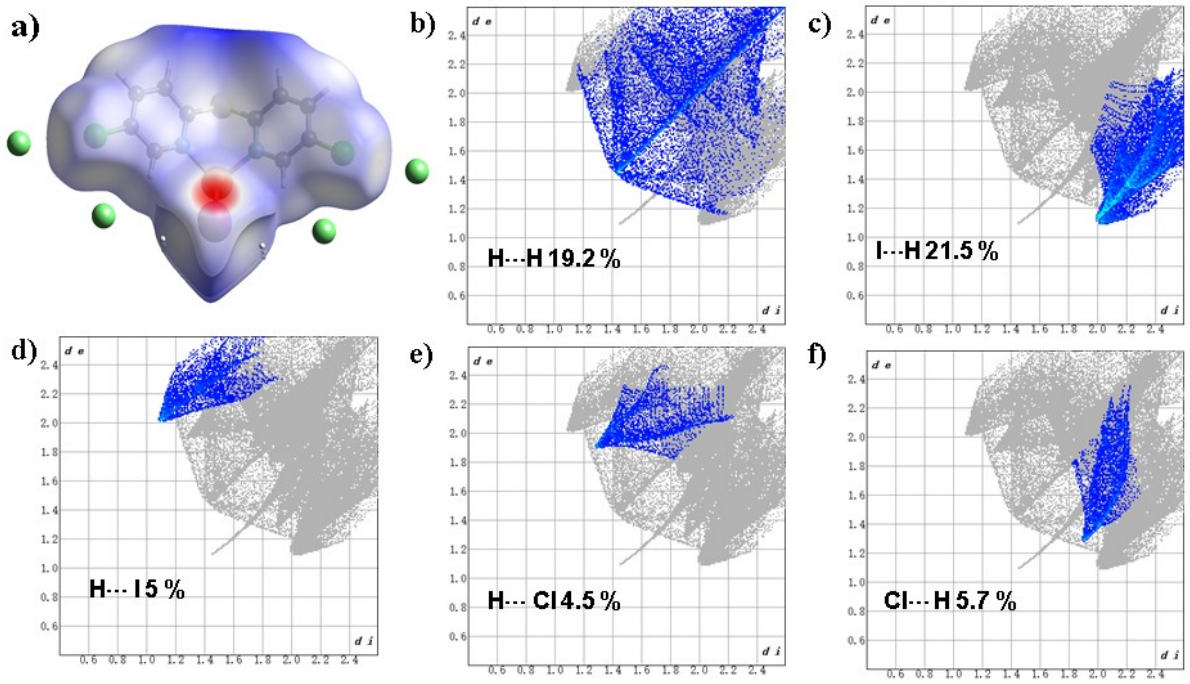

Fig. S4 (a) Hirshfeld surface of one repeating unit of **BCS-CuI** showing the contact Cl atoms. The red area on the top and bottom of the surface correspond with the Cu–I coordination bonds within the chain. (b-f) The 2D fingerprint for **BCS-CuI** showing different contributions from non-covalent interactions of H···H, I···H, H···I, H···Cl and Cl···H.

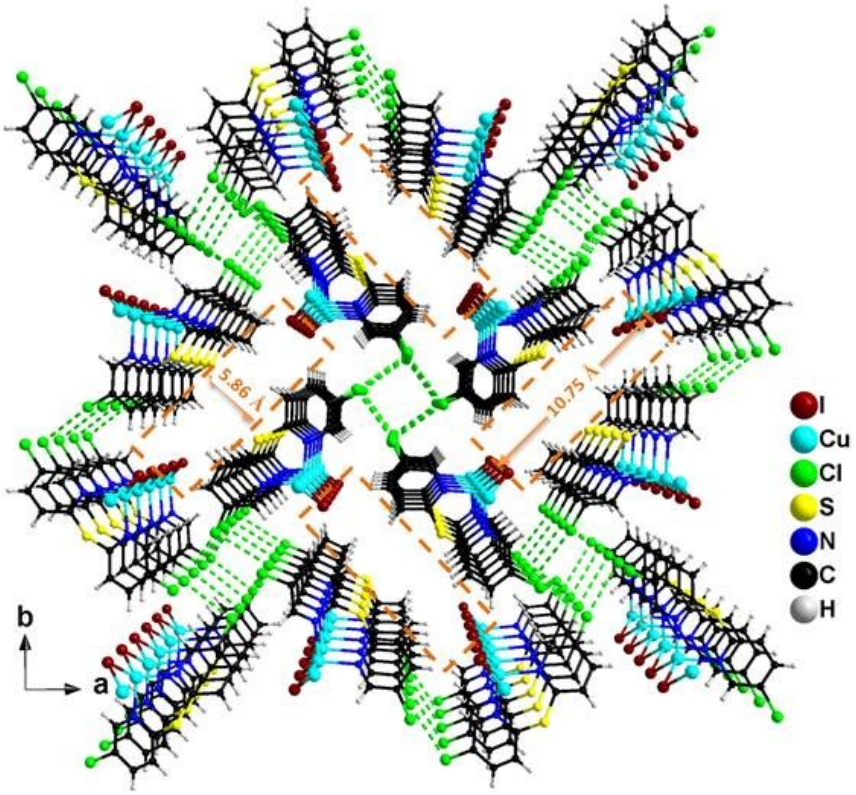

Fig. S5 Demonstration of the rectangular channels formed by the Cl···Cl interactions between hybrid chains of **BCS-CuI**.

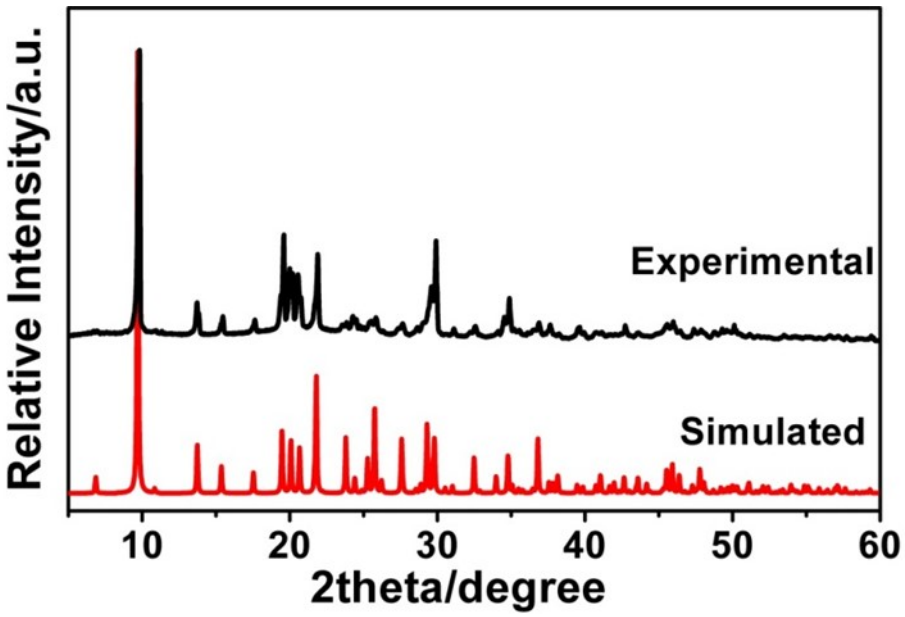

Fig. S6 The experimental and simulated PXRD patterns of **BCS-CuI**.

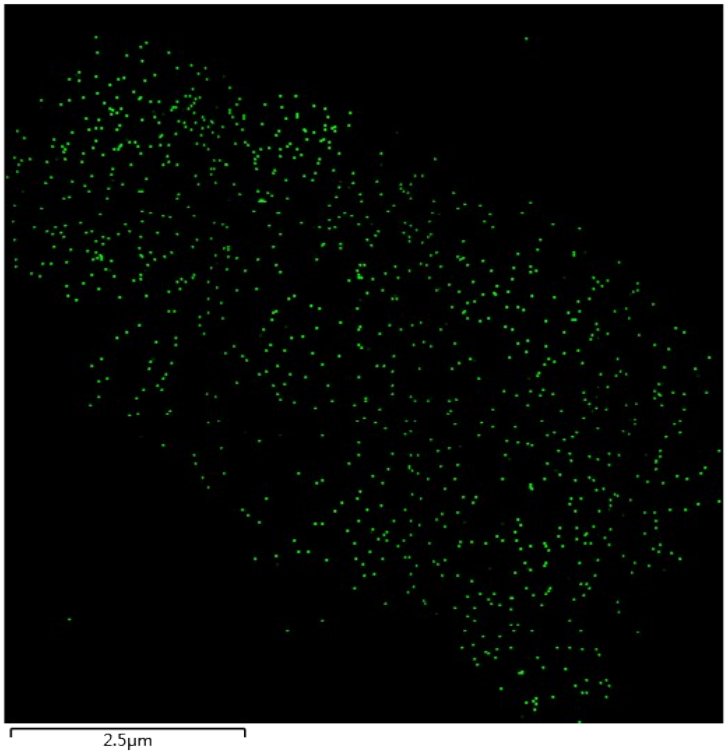

Fig. S7 The I element mapping analysis.

Table S5 Photographs, crystal data and structure refinement for single crystals of BCS-CuI after 75% moisture treated [denoted as BCS-CuI (75% RH)] and 254 nm UV light irradiation for 1 month [denoted as BCS-CuI (UV)].

Crystal	**BCS-CuI (75% RH)**	**BCS-CuI (UV)**
Morphology	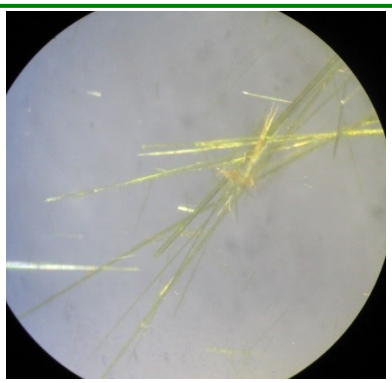	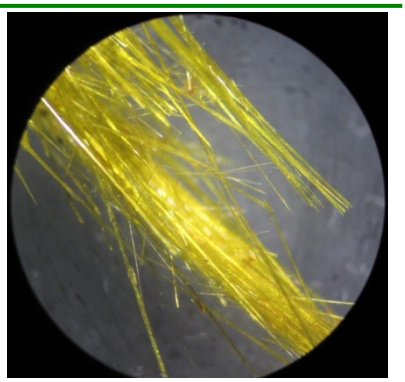
Diffraction indexing rate/%	90.2	95.2
a, b, c/ Å	18.24(1), 18.24(1), 4.20(1)	18.24(1), 18.24(1), 4.21(1)
α, β, γ/°	90, 90, 90	90, 90, 90
GOOF	0.960	0.991
R_1[a], wR_2[b] [I>2s(I)]	0.083, 0.1117	0.059, 0.078
$\Delta\rho_{max}$ and $\Delta\rho_{min}$ [e Å^{-3}]	1.30, –0.68	0.69, –1.09
Distance (Cu–I)/ Å	2.562-2.628	2.557-2.636
Distance (Cu–N)/ Å	2.064	2.059
Distance (C–S)/ Å	1.778	1.781

Brief discussion for stability evaluation:

The morphology monitoring reveals that the single crystals after moisture and UV light treatments still remain glittering and translucent, indicating their well single crystallinity. The SXRD experiment results for the random selected single crystals are summarized. They both have excellent structural refinement results and have similar cell parameters, bond distances and bond angles as the as-synthesized crystals.

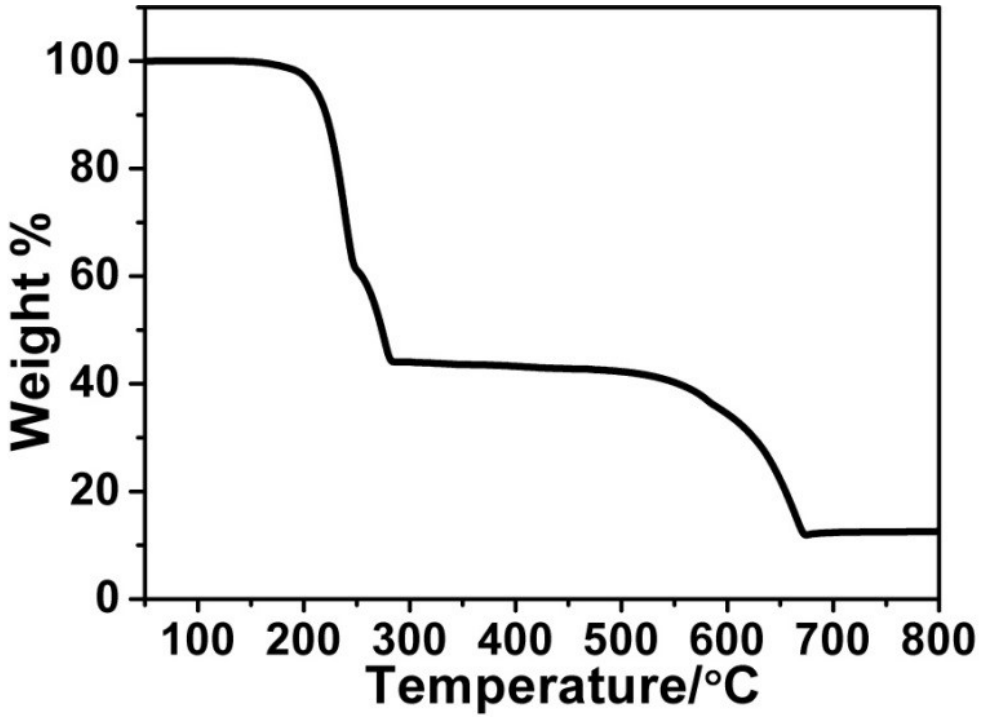

Fig. S8 TGA curve of **BCS-CuI**.

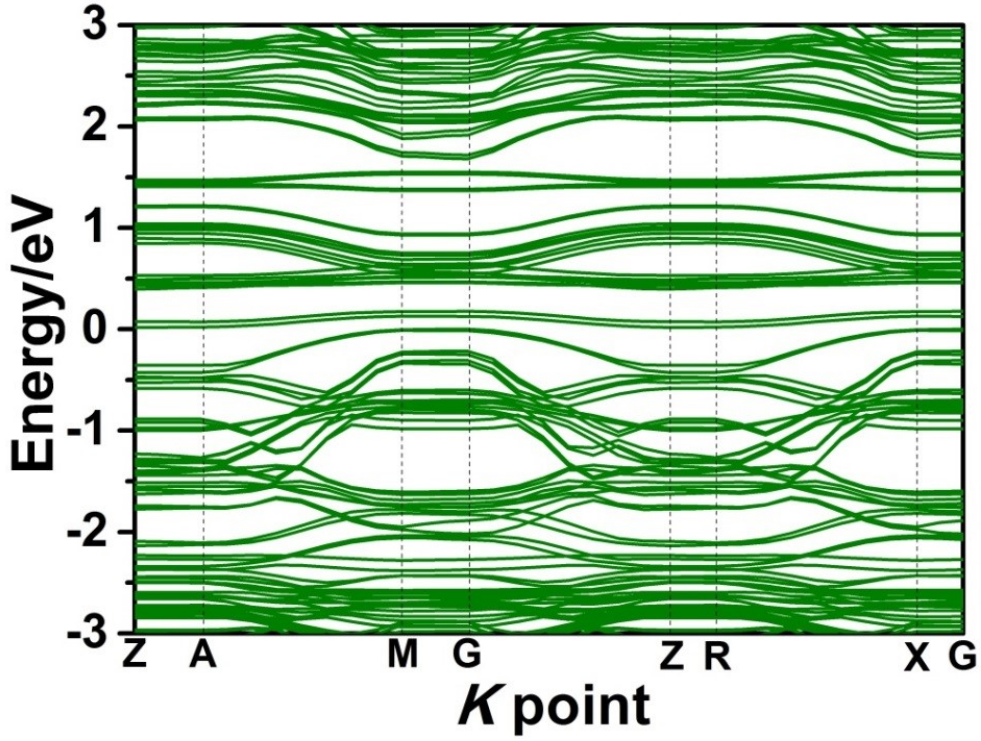

Fig. S9 Electronic band structure of **BCS-CuI**, where the VBM and CBM locate at the different *K* point.

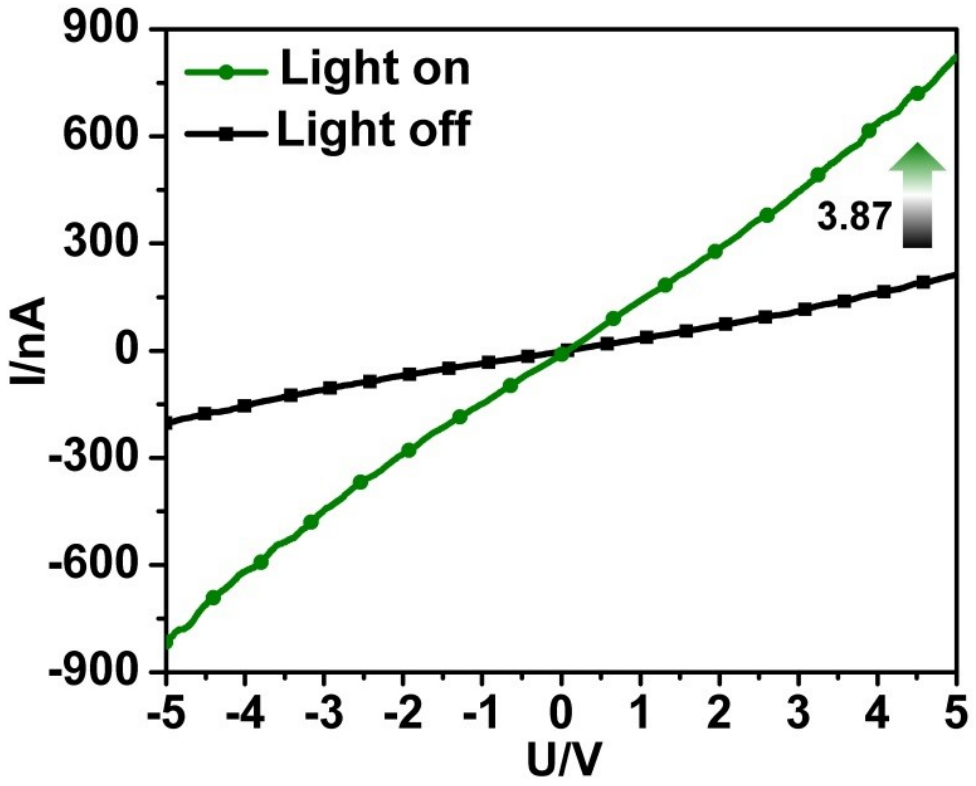

Fig. S10 I−V curve for the film device of $MA_3Bi_2I_9$ in the dark and under Xe lamp illumination. The tests were performed under the same condition as that for **BCS-CuI** film.

Table S6 Comparison of the Photodetection Device Parameters.

Material	Device type	Resistance (Ω)	Response range (nm)	On/off ratio	Eg (eV)	Reference
BCS-CuI	Thin film	2.60×10^{10}	400-700	32.9	2.44	This work
$K_2Cu_2Cl_6$	Thin film	NA	330-390	1.9	1.85	20
$CsCuCl_3$	Thin film	2.9×10^{4}	369	30	1.92	21
$CuBiI_4$	Thin film	NA	532	2.2	1.84	22
$Cs_3Cu_2I_5$	Thin film	1×10^{6}	265/365	127	3.8	23
$F_{16}CuPc$	Nanoflake	NA	300	1.9×10^{6}	NA	24
$CuSbS_2$	Nanocrystals	7.6×10^{7}	300-600	5	1.38-1.52	25
$[Cu_6I_3(TP)_3(CH_3CN)_2]_n$	NA	8.3×10^{5}	NA	NA	1.98	26
$(Mebtz)_2Cu_3I_5$	Thin film	2.92×10^{3}	White light	35.4	2.4	27

Pc = phthalocyanine; TP = thiophenol; Mebtz = methylbenzothiazole.

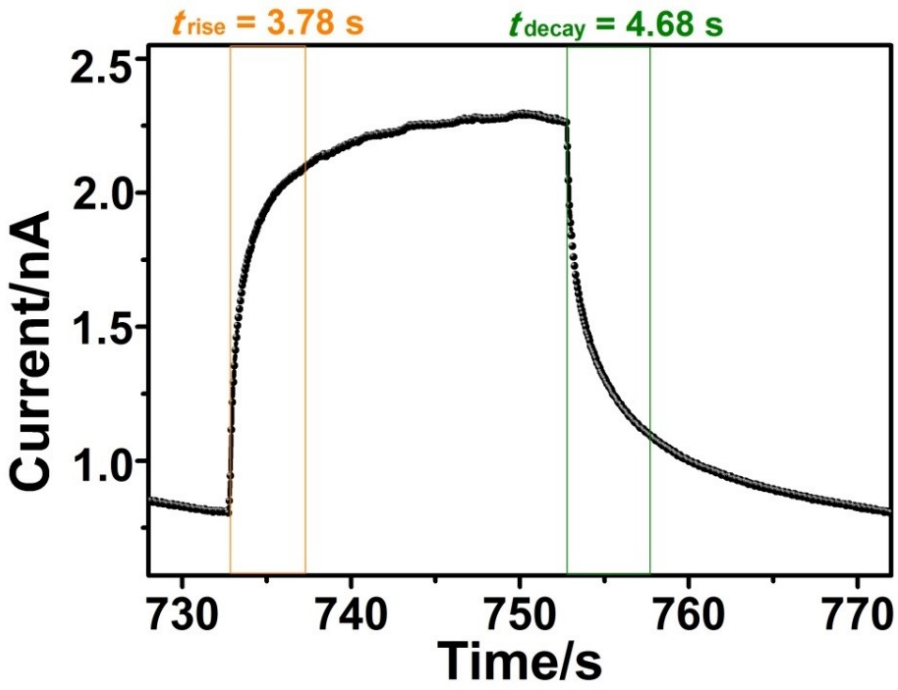

Fig. S11 Temporal photocurrent response showing a rise and a decay time for the film device of **BCS-CuI**. The rise and fall times were defined as the time required for the current increasing from 10% to 90% and decreasing from 90% to 10%.

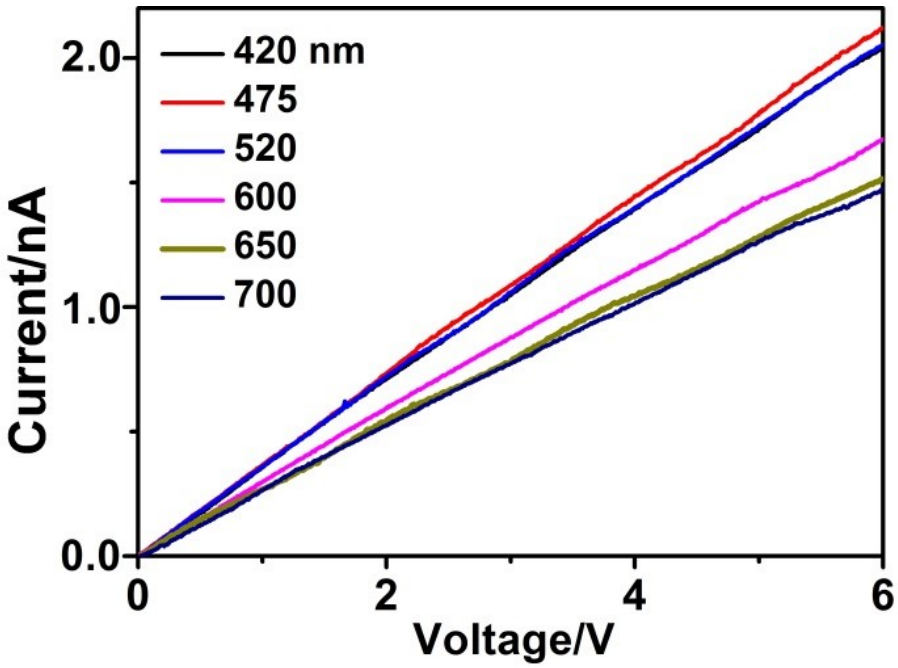

Fig. S12 I-V curves of the thin film device for **BCS-CuI** under selected monochromatic light irradiation with a fixed light intensity of 10 mW·cm^{-2}.

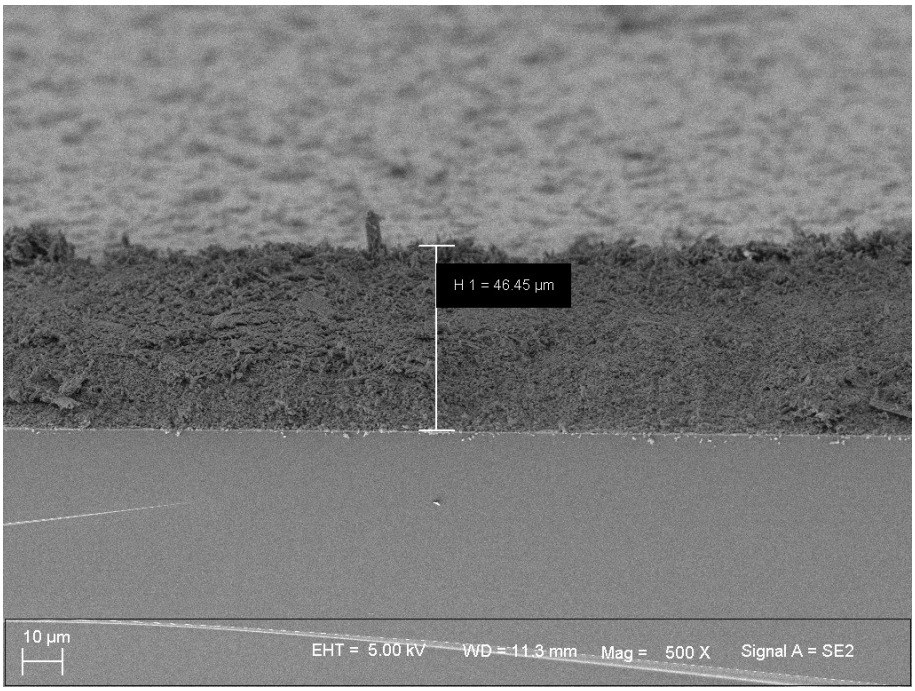

Fig. S13 SEM image of the BCS-CuI film used for the Hall measurement.

Table S7 Summary of the E_b Values of Selected Metal Halides.

Material	Dimension	E_b/ meV	Method	Reference
BCS-CuI	1D	55.8	Temperature-dependent PL	This work
$Cs_3Cu_2I_5$	0D	490	Temperature-dependent PL	28
$MAPbI_3$	3D	45	Temperature-dependent PL	29
$FAPbI_3$	2D	35	Calculation	30
$(NH_2Cl{=}NH_2)_3PbI_5$	1D	715 ≥ 410	Calculation Optical absorption	31
$MA_3Bi_2I_9$	0D	300	Optical absorption	32
$Cs_3Sb_2I_9$	0D	166	Temperature-dependent PL	33

FA = formamidinium ($HC(NH_2)_2^+$)

Table S8 Summary of the Carrier Mobility values of Selected Metal Halides.

Material	**Architecture**	**Carrier type**	**Carrier mobility/cm^2·V^{-1}·s^{-1}**	**Carrier concentration/cm^{-3}**	**Method**	**Reference**
BCS-CuI	Film	Electron	555	1.73×10^{11}	Hall	This work
$Cs_3Cu_2I_5$	Film	Electron/hole	0.828/0.036	NA	SCLC	23
$MAPbI_3$	Pellet	Electron	66	1×10^{9}	Hall	34
$MASnI_3$	Pellet	Hole	2320	1×10^{14}	Hall	34
$FAPbI_3$	Film	Electron/hole	27	NA	TRTS	35
$MA_3Bi_2I_9$	Film	Hole	18	3.36×10^{18}	Hall	36
$(NH_4)_3Sb_2I_9$	Film	Electron/hole	12.3/4.8	NA	SCLC	37

TRTS: Time-resolved THz spectroscopy; SCLC: Space charge limited current method.

References:

1. W. M. Wendlandt and H. G. Hecht, *Reflectance Spectroscopy*. Interscience: New York, 1966.
2. M. J. Turner, J. J. McKinnon, S. K. Wolff, D. J. Grimwood, P. R. Spackman, D. Jayatilaka and M. A. Spackman CrystalExplorer17. https://hirshfeldsurface.net.
3. K. Wu, A. Bera, C. Ma, Y. Du, Y. Yang, L. Li and T. Wu, *Phys. Chem. Chem. Phys.*, 2014, **16**, 22476-22481.
4. M. D. Segall, P. J. D. Lindan, M. J. Probert, C. J. Pickard, P. J. Hasnip, S. J. Clark and M. C. Payne, *J. Phys.: Condens. Matter*, 2002, **14**, 2717-2744.
5. V. Milman, B. Winkler, J. A. White, C. J. Pickard, M. C. Payne, E. V. Akhmatskaya and R. H. Nobes, *Int. J. Quantum Chem.*, 2000, **77**, 895-910.
6. D. R. Hamann, M. Schluter and C. Chiang, *Phys. Rev. Lett.*, 1979, **43**, 1494-1497.
7. Agilent, *CrysAlisPro*. Version 1.171.35.21 ed.; Agilent Technologies Corp.: California, America.
8. Siemens, *SHELXTL Version 5 Reference manual*. Siemens Energy & Automaion Inc.: Madision,WI, 1994.
9. Z. Lian, B. N. Bhawal, P. Yu and B. Morandi, *Science*, 2017, **356**, 1059-1063.
10. K. Mitamura, T. Yatabe, K. Yamamoto, T. Yabe, K. Suzuki and K. Yamaguchi, *Chem. Commun.*, 2021, **57**, 3749-3752.
11. S. G. Modha, V. P. Mehta and E. V. Van der Eycken, *Chem. Soc. Rev.*, 2013, **42**, 5042-5055.
12. L. D. Wang, W. He and Z. K. Yu, *Chem. Soc. Rev.*, 2013, **42**, 599-621.
13. C. Uyeda, Y. Tan, G. C. Fu and J. C. Peters, *J. Am. Chem. Soc.*, 2013, **135**, 9548-9552.
14. M. S. Oderinde, M. Frenette, D. W. Robbins, B. Aquila and J. W. Johannes, *J. Am. Chem. Soc.*, 2016, **138**, 1760-1763.
15. K. D. Jones, D. J. Power, D. Bierer, K. M. Gericke and S. G. Stewart, *Org. Lett.*, 2018, **20**, 208-211.
16. T. Sugahara, K. Murakami, H. Yorimitsu and A. Osuka, *Angew. Chem., Int. Ed.*, 2014, **53**, 9329-9333.
17. M. Tobisu, Y. Masuya, K. Baba and N. Chatani, *Chem. Sci.*, 2016, **7**, 2587-2591.
18. Y. H. Ma, J. Cammarata and J. Cornella, *J. Am. Chem. Soc.*, 2019, **141**, 1918-1922.
19. T. Delcaillau, A. Bismuto, Z. Lian and B. Morandi, *Angew. Chem., Int. Ed.*, 2020, **59**, 2110-2114.
20. H. Zhou, X. Liu, G. He, L. Fan, S. Shi, J. Wei, W. Xu, C. Yuan, N. Chai, B. Chen, Y. Zhang, X. Zhang, J. Zhao, X. Wei, J. Yin and D. Tain, *ACS Omega*, 2018, **3**, 14021-

14026.
21. S. Cui, Y. Chen, S. Tao, J. Cui, C. Yuan, N. Yu, H. Zhou, J. Yin and X. Zhang, *Eur. J. Inorg. Chem.*, 2020, **2020**, 2165-2169.
22. N. Qu, Y. Lei, X. Yang, X. Hu, W. Zhao, C. Zhao and Z. Zheng, *J. Mater. Chem. C*, 2020, **8**, 8451-8456.
23. Z.-X. Zhang, C. Li, Y. Lu, X.-W. Tong, F.-X. Liang, X.-Y. Zhao, D. Wu, C. Xie and L.-B. Luo, *J. Phys. Chem. Lett.*, 2019, **10**, 5343-5350.
24. H. Yan, Y. Li, J.-K. Qin, P. A. Hu, L. Zhen and C.-Y. Xu, *Adv. Opt. Mater.*, 2019, **7**, 1901097-1901104.
25. M. Hao, Y. Liu, F. Zhou, L. Jiang, F. Liu and J. Li, *ECS Solid State Lett.*, 2014, **3**, Q41-Q43.
26. Y. Sun, M. Amsler, S. Goedecker, A. Caravella, M. Yoshida and M. Kato, *CrystEngComm*, 2019, **21**, 3948-3953.
27. R.-Y. Zhao, G.-N. Liu, Q.-S. Liu, P.-F. Niu, R.-D. Xu, Z.-H. Wang, T.-H. Wei, J. Zhang, Y.-Q. Sun and C. Li, *Cryst. Growth Des.*, 2020, **20**, 1009-1015.
28. T. Jun, K. Sim, S. Iimura, M. Sasase, H. Kamioka, J. Kim and H. Hosono, *Adv. Mater.*, 2018, **30**, 1804547.
29. T. Ishihara, *J. Lumin.*, 1994, **60**, 269-274.
30. A. Miyata, A. Mitioglu, P. Plochocka, O. Portugall, J. T.-W. Wang, S. D. Stranks, H. J. Snaith and R. J. Nicholas, *Nat. Phys.*, 2015, **11**, 582-U94.
31. I. B. Koutselas, L. Ducasse and G. C. Papavassiliou, *J. Phys. Condens. Matter*, 1996, **8**, 5953-5953.
32. T. Kawai, A. Ishii, T. Kitamura, S. Shimanuki, M. Iwata and Y. Ishibashi, *J. Phys. Soc. Jpn.*, 1999, **65**, 1464-1468.
33. J. P. Correa-Baena, L. Nienhaus, R. C. Kurchin, S. S. Shin, S. Wieghold, N. T. P. Hartono, M. Layurova, N. D. Klein, J. R. Poindexter, A. Polizzotti, S. J. Sun, M. G. Bawendi and T. Buonassisi, *Chem. Mater.*, 2018, **30**, 3734-3742.
34. C. C. Stoumpos, C. D. Malliakas and M. G. Kanatzidis, *Inorg. Chem.*, 2013, **52**, 9019-9038.
35. W. Rehman, R. L. Milot, G. E. Eperon, C. Wehrenfennig, J. L. Boland, H. J. Snaith, M. B. Johnston and L. M. Herz, *Adv. Mater.*, 2015, **27**, 7938-7944.
36. X. Chen, Y. Myung, A. Thind, Z. Gao, B. Yin, M. Shen, S. B. Cho, P. Cheng, B. Sadtler, R. Mishra and P. Banerjee, *J. Mater. Chem. A*, 2017, **5**, 24728-24739.
37. C. Zuo and L. Ding, *Angew. Chem., Int. Ed.*, 2017, **56**, 6528-6532.